ANALYZING THE SENSITIVITY OF HAIL PREDICTION TO MODEL GRID SPACING

Tyler Green
Embry-Riddle Aeronautical University, Daytona Beach, Florida

Nathan Snook
Center for Analysis and Prediction of Storms, Norman, Oklahoma

Amy McGovern
School of Computer Science, University of Oklahoma, Norman, Oklahoma

National Weather Center Research Experiences for Undergraduate Program
Norman, Oklahoma

Center for Analysis and Prediction of Storms, University of Oklahoma, Norman, Oklahoma

ABSTRACT

At grid spacings of 1 kilometer or less, there has been little to no research on possible sensitivities of hail prediction to model gird spacing using ensemble modeling. Research on sensitivities of hail at fine grid spacings (500 meters or less) will be important for future operational products, as one of Warn on Forecast's goals is short term prediction of hail using ensemble modeling. In this study, three ensemble runs using horizontal grid spacings of 500, 250, and 100 meters were analyzed to find systematic differences in explicitly predicted model hail using a Milbrandt and Yau double moment bulk microphysical scheme. Hail and hail related fields were investigated to identify sensitivities as horizontal gird spacing was changed and whether hail related fields such as distribution of updrafts and graupel could help to explain potential sensitivities. Systematic differences were identified in the mass of hail field, with increased spatial coverage of large hail mass values at select vertical levels as grid spacing was decreased. Particle size distributions indicate the increase in spatial distribution of high hail mass is accompanied with an increase in concentration of large diameter hailstones. Differences in updraft distribution and near storm environment did not prove to account for differences found in the mass of hail field. However, distributions of mass of graupel suggest that a microphysical budget analysis is needed to explain sensitivities in the mass of hail field as horizontal grid spacing is decreased.

1. Introduction

As the grid spacing of experimental and operational models used to predict severe weather hazards continue to decrease, the sensitivity of storm processes to grid resolution must be considered. Initial studies of these sensitivities will be important in guiding future sub-kilometer scale convective modeling studies.

Hail is a severe weather hazard that causes over a billion dollars in damages each year in the United States (Allen 2017). Occasionally, damage costs from a single hail storm can exceed

Corresponding author address: Tyler Green, Embry-Riddle Aeronautical University, 600 S Clyde Morris Blvd, Daytona Beach, Florida 32114

$1 billion dollars. In one recent example, the May 2017 Denver and April 2016 North/Central Texas hail storms caused $2.2 billion an $3.6 billion in total estimated costs respectively (NOAA, 2017).

Compared to other severe weather hazards such as tornados, wind, and flooding, explicit prediction of hail has not been extensively studied, particularly for sub-kilometer scale ensemble forecast studies (Snook et al. 2016). Previous studies have considered the sensitivity of mesocyclone development to model grid spacing (Adlerman and Droegemeier 2002), grid spacing requirements for resolving deep moist convection (Bryan et al 2003), and explicit prediction of tornados (Orf, 2017). However, a literature review suggests that there has yet to be a study focused on the sensitivity of hail prediction to model grid spacing in models with horizontal grid spacing of less than one kilometer.

Currently, HAILCAST, a one dimensional coupled cloud and hail model, can be used operationally by the Storm Prediction Center to forecast the maximum expected hail diameter at the surface (Adams-Selin and Ziegler 2016). HAILCAST, which originally used a one dimensional cloud model, was modified by Adams-Selin and Ziegler (2016) to use a one-way coupling of three-dimensional model output from the Weather Research and Forecasting Model (WRF) with HAILCAST. This one-way coupling provides more physically realistic data to HAILCAST than the one-dimensional cloud model that was originally used (Adams-Selin and Ziegler 2016). Short term prediction of hail using high resolution models such as WRF is one of the goals of NOAA's warn-on-forecast system (Stensrud et al. 2009). Compared to HAILCAST, prediction of hail directly from microphysical NWP is less prone to the introduction of error caused by coupling with an external hail model, and if hail can be explicitly predicted by the model microphysics, it would eliminate the need for an external model. Furthermore, analyzing the changes in explicitly predicted model hail as grid spacing is varied over a range of sub-kilometer grid spacings will be important for the development of these models, particularly with regard to the model microphysics, and will be valuable guidance for future operational

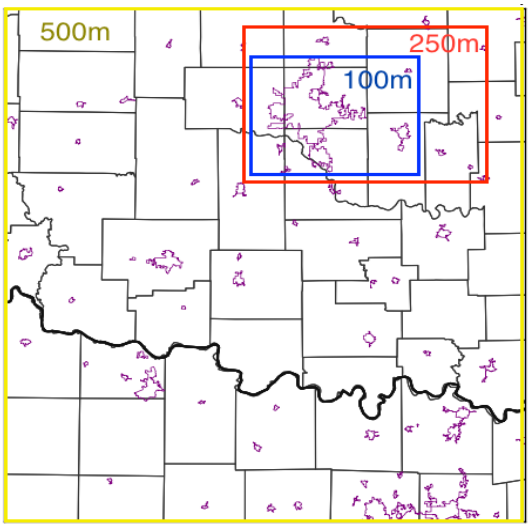

Figure 1: Model domains for three grid spacings used. Purple outlines indicate urban areas while light black outlines represent county outlines. The larger urban area inside the 100m domain represents the OKC urban area. Colors associated with the specific grid spacings are used consistently in figures throughout this paper.

implementations as grid spacing continues to decrease.

The microphysical schemes used in today's models are very complex and require numerical approximations for many interactions inside clouds (Stensrud 2007). Because of these assumptions and the use of imperfect observations (Stensrud 2007), it is imperative to document how these schemes behave in terms of hail production when model grid spacing is decreased to be able to resolve small, sub-storm scale features. Consequently, the purpose of this paper is to explore, identify, and document the differences in hail prediction and hail related variables due to changes in model grid spacing.

2. Data and Methods

In this paper, the May 20 2013 supercell that produced the EF5 Newcastle-Moore tornado will be the primary focus, as it produced numerous reports of severe hail (Snook et al 2016). For more information on the storms of 20 May 2013

the reader is referred to Zhang et al. (2015). The Advanced Regional Prediction System and its EnKF DA system (Xue et al. 2006; Tong and Xue 2008 was used to produce three forecast ensembles with horizontal grid spacings of 500, 250, and 100 meters, with each ensemble consisting of 40 members. The model settings largely follow Snook et al. (2015): radiation is parameterized using the NASA Goddard Space Flight Center long and shortwave parameterization, a two-layer soil model, sub grid turbulence is parameterized using a 1.5-order turbulent kinetic energy based scheme. For more information on the model settings we refer the reader to Snook et al (2015) and Snook et al (2016).

The 500-meter model domain consists of a 603×653×63 grid that covers much of Oklahoma and part of northern Texas (Snook et. al 2016). The 250-meter model domain consists of a 399×563×63 grid located in the northeastern portion of the 500-meter domain. The 100-meter model run uses a 722×1002×63 grid very similar (although slightly smaller in geographic extent) to the 250-meter domain. These three model domains are plotted in **Figure 1**. A stretched vertical grid is used, with grid spacing being the smallest near the surface and increasing with height (Snook et al. 2016). The 500m and 250m runs have minimum vertical spacing of 50m at the surface while the 100m run has a minimum vertical spacing of 20m at the surface. The average vertical grid spacing for the 500m and 250m runs is 425m while for the 100m run the average vertical grid spacing is 340m. In this study, all comparisons are made using a sub-domain corresponding to the extent of the 100-meter grid.

All three model forecasts use the Milbrandt and Yau (2005) microphysical parameterization scheme where the hydrometeor particle size distribution is represented by a gamma function:

$$N(D) = N_0 D^{\alpha} e^{-\lambda D} \qquad (1)$$

where $N(D)$ is the number of particles of a given diameter, and $N_0, \alpha,$ and λ are the intercept, shape, and slope parameters respectively (Snook et al. 2016). The forecasts being used for this study used a shape parameter of zero. The two-moment microphysical scheme better represents the size sorting and melting for hail than a single moment scheme, which allows it to more accurately represent the true processes that affect hail production (Snook et al. 2016).

The goal of this study was to find and document systematic differences in hail prediction across the three model grid spacings being tested, and explore the causes for the systematic differences observed. To accomplish this, several different variables related to hail will be compared across the three model runs which use horizontal grid spacing ranging from 500 to 100 meters. These variables are discussed below.

a. Mass of Hail

The model, through the two-moment Milbrandt and Yau microphysics scheme, explicitly predicts the number concentration and mixing ratio of hail within each model grid volume, therefore the mass of hail per cubic meter can be obtained for each grid volume by taking the product of the hail mixing ratio and air density as shown below.

$$m_h = q_h * \rho_{air} \qquad (2)$$

Mass of hail will be the most extensively studied variable in this paper and will be analyzed qualitatively through swaths and cross sections, and quantitatively through histograms, Kolmogorov-Smirnov statistical tests, and total mass versus time diagrams. Swaths and cross sections are examined to identify differences in structure and intensity of hail mass. Histograms are made at three vertical levels including near the surface, near freezing level, and at 6 kilometers above the surface (well above the freezing level) to identify differences in the amount and distribution of hail mass at different levels of the storm. Statistical analyses of hail mass distribution will be performed to determine if differences are statistically significant. Total mass versus time diagrams are utilized to get an overview of total mass of hail being produced, to compare to the histograms which only analyze distributions at three vertical levels.

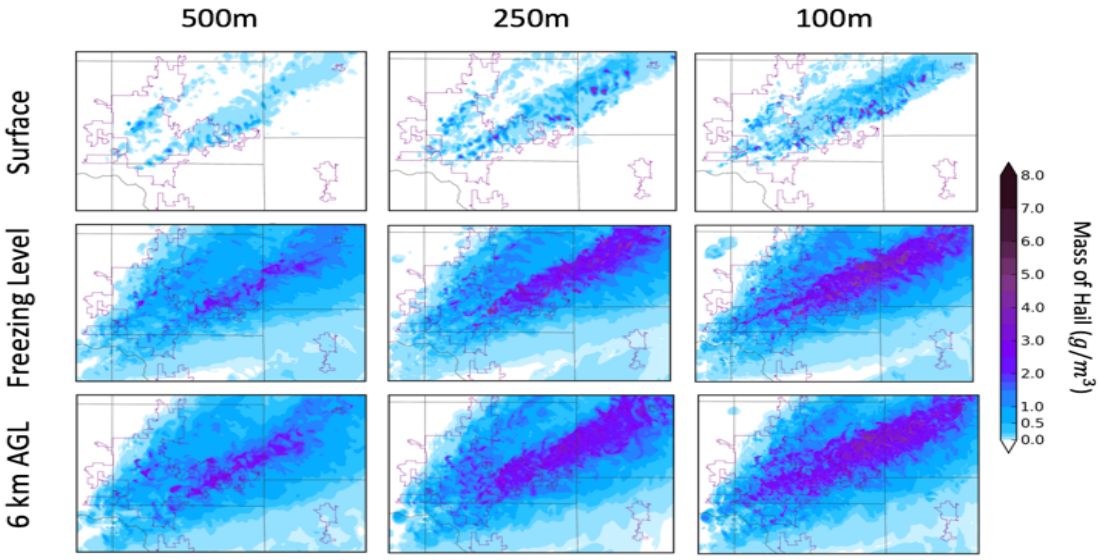

Figure 1: 2D mass of hail swaths for ensemble member 19.

b. Hail Mean Mass Diameter and Particle Size Distribution

The mass of hail field does not give information about the distribution of different hailstone sizes. Mean mass diameter (hereafter referred to as MMDI) and particle size distribution (hereafter referred to as PSD) are derived variables from the output of the model microphysics that give representations of hailstone diameter and concentrations of different diameter hailstones respectively. MMDI will be analyzed through the use of cross sections similar to those made for mass of hail. From the model predicted slope parameter and intercept parameter, a PSD curve in the form of equation (1) can be plotted. For a specific ensemble member and grid spacing, the maximum mass of hail is found within the domain and the two previously mentioned parameters are averaged from time 6000 to 9000s to obtain one PSD curve. Therefore, for one ensemble member and vertical model level, 3 PSD curves will be plotted so a comparison of the curves can be made.

c. Distribution of Updrafts and Near Storm Environment

The intensity, size, and location of updrafts are important in hail production and determining how large hailstones can grow, with stronger, more vertically-oriented updrafts correlated with larger hailstones. Distribution of updrafts at the freezing level and the 6 km level along with Kolmogorov-Smirnov statistical test are made to analyze the distribution of updrafts.

Horizontal plots of surface based convective available potential energy (CAPE) will be compared across grid spacings to analyze temporal differences in the near storm environment. Differences in CAPE could cause differences in updraft speeds, as larger values of CAPE can correspond to larger accelerations for updrafts. Therefore, differing values of cape in the near storm environment ahead of the supercell could affect the spatial distribution of updraft speeds in the supercell.

d. Distribution of Mass of Graupel

Graupel is an important hail related variable because graupel serves as the embryos for hailstones (Stensrud 2007). The distribution of graupel is therefore analyzed via histograms and statistical tests at the freezing and 6 km vertical levels to identify any differences between the graupel mass and hail mass fields. Differences between these two fields could indicate differences in the microphysical processes which are beyond the scope of this paper.

3. Results

a. 2D Swaths of Hail Mass

One of the most direct qualitative methods for analyzing the mass of hail field is swaths of maximum hail mass at the surface over the entire forecast period. Swaths were produced for all ensemble members at all three grid spacings (500m, 250m, and 100m) to investigate systematic differences in the intensity and spatial coverage of hail at the surface, near the freezing level, and at 6 km above the surface (well above the freezing level). In **Figure 2**, the difference in intensity and structure of the hail swaths are plotted for ensemble member 19, an ensemble member that produced large amounts of hail mass at the surface. The 500m forecast produces less total coverage of hail at the surface than the 250m and 100m forecasts, and the most intense areas of hail in the 500 m forecast are less widespread and exhibit lower maximum values compared to the 250m and 100m forecasts. Compared to the 250m hail mass swath, the 100m swath contains more highly-localized areas of high hail mass (> 4 g m^{-3}) at the surface. Maximum hail mass in the 100m swath at the surface is higher, exceeding 6 g m^{-3}, compared to a maximum of less than 5.5 g m^{-3} in the 250m swath.

A similar trend can be seen in the hail mass swaths at the freezing level and the 6 kilometer level in **Figure 2**. Noticeably, there is more geographic coverage of low hail mass at these levels than at the surface, as much of small hail on the northern and southern edge of the upper level swaths melts before it reaches the ground. The maximum areas of hail in the 100m swath are more concentrated compared to the 250m swath, however there is greater geographic coverage of moderate hail mass (2.5-4.0 g m^{-3}) at the freezing and 6 kilometer levels. These trends are considered quantitatively in the following section through the use of area-weighted histograms and statistical significance tests.

b. Mass of Hail Histograms

To analyze the geographic distribution of hail mass, histograms are produced for the levels used above in section 2 using data from all ensemble members at all times during the forecast period—these histograms are plotted in **Figure 3**. It is important to note that the histograms in **Figure 3** are not pure histograms (in the sense that the y axis represents a frequency), but instead represent the total frequency of a certain range of hail masses multiplied by the area of a single grid cell at each grid spacing (e.g. the square of the horizontal grid spacing in meters), in order to account for the different size of grid cells in the three ensembles and accurately represent the total geographic coverage for each range of hail masses. It is also important to note that the histograms in **Figure 3** are plotted on a logarithmic scale in the vertical. Hail mass bins are spaced at intervals of 0.1 g m^{-3} in the horizontal.

For all three vertical levels, the 100m forecast produces greater geographic coverage of hail across almost all mass bins compared to the 250m and 500m forecasts, with exceptions in the very low hail mass ranges where the geographic coverage is similar for all three grid spacings. Another exception is for moderate hail masses (0.5-3.0 g m^{-3}) in the freezing level histogram, where the 250m ensemble produces slightly more geographic coverage than the 500m ensemble. In all three histograms, the 100m ensemble produces larger maximum hail masses than the 250m and 500m ensembles, and the 250m ensemble produces larger maximum hail masses than the 500m ensemble. This suggests that, as the grid spacing decreases, the largest hail masses produced within the model microphysics scheme increases. These histograms also suggest that as the grid spacing is decreased, the geographic coverage of relatively high hail mass (> 4.0 g m^{-3}) likewise increases.

To test the statistical significance of these results, a two distribution Kolmogorov-Smirnov test (hereafter referred to as KS2 test) was performed to compare the distributions of the 500m, 250m, and 100m ensembles for designated ranges of hail mass: 0.0-2.0, 2.0-4.0, 4.0-6.0, and 6.0-9.0 g m^{-3}. The KS2 test was performed at the same set of three vertical levels as the histograms, and are shown below the corresponding histograms in **Figure 3**. A commonly accepted p value that determines if two distributions are significantly different is 0.05, which is the value that will be used in these tests.

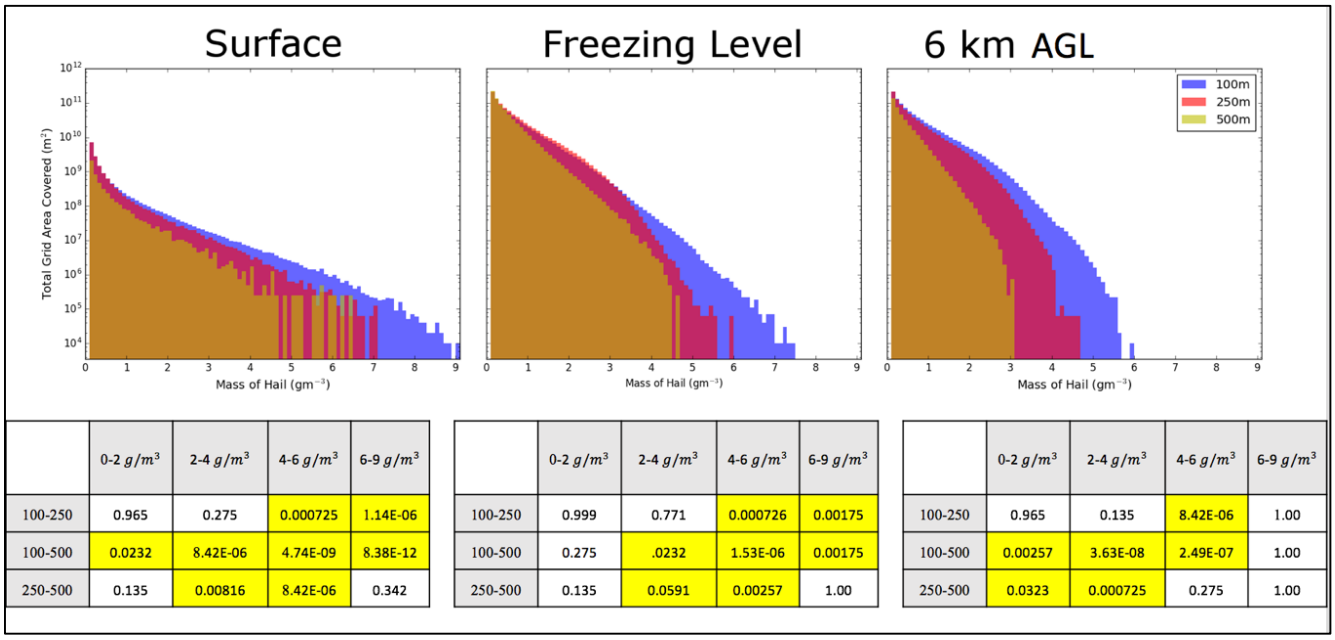

	0-2 g/m^3	2-4 g/m^3	4-6 g/m^3	6-9 g/m^3
100-250	0.965	0.275	0.000725	1.14E-06
100-500	0.0232	8.42E-06	4.74E-09	8.38E-12
250-500	0.135	0.00816	8.42E-06	0.342

	0-2 g/m^3	2-4 g/m^3	4-6 g/m^3	6-9 g/m^3
100-250	0.999	0.771	0.000726	0.00175
100-500	0.275	.0232	1.53E-06	0.00175
250-500	0.135	0.0591	0.00257	1.00

	0-2 g/m^3	2-4 g/m^3	4-6 g/m^3	6-9 g/m^3
100-250	0.965	0.135	8.42E-06	1.00
100-500	0.00257	3.63E-08	2.49E-07	1.00
250-500	0.0323	0.000725	0.275	1.00

Figure 3: Mass of hail histograms for surface, freezing level, and 6 kilometers AGL. Hail mass bins are spaced at intervals of 0.1 g m^{-3} in the horizontal. Corresponding table of p values from Kolmogorov-Smirnov test shown below histograms.

At the surface, the 100m distribution is significantly different from the 500m distribution across all hail masses. The difference between the 100m and 250m distributions is not statistically different for the 0.0-4.0 g m^{-3} range, though the difference is significant for higher hail masses. The 250m and 500m distributions are only significantly different in the 2-6 g m^{-3} range.

Similar statistical properties are present at the freezing level. The 500m and 100m distributions are significantly different for all hail masses greater than 2 g m^{-3}, and the 100m and 250m distributions are, just as at the surface, significantly different for hail masses greater than 4 g m^{-3}. The 250m and 500m distributions are again statistically different only in the range of 2.0-6.0 g m^{-3}. Note that the p-values of 1.00 seen for some ranges in the freezing level and 6 km level tests are caused by no data for either distribution existing at that range of hail masses.

The 6-9 g m^{-3} range will not be considered at the 6 km level, because hail in that range was not produced in any of the three grid spacings. At 6 km, however, the 100m and 500m distributions show significant differences across all hail masses, while the 100m and 250m distributions only exhibit significant difference in the 4-6 g m^{-3} range. The 250m and 500m distributions show significant difference for the 0.0-4.0 g m^{-3} range.

From the histograms and statistical analysis of the mass of hail distributions, it is apparent that as the grid spacing decreases, the distributions of larger hail masses (4.0-9.0 g m^{-3}) are significantly different in that the forecasts with smaller grid spacings are producing more geographic coverage of hail in that 4.0-9.0 g m^{-3} range. The histograms in **Figure 3** also suggest that the smaller grid spacing forecasts are melting less of the larger hail than the larger grid spacings are based on distributions of hail mass at these three levels.

c. Domain-wide Hail Mass as a Function of Time

In the previous section, differences between the distributions of hail mass at 3 specific vertical model levels were discussed. In this section, we will consider total mass produced by an ensemble member as a function of time for several selected ensemble members to examine differences in the total hail mass produced rather than focusing exclusively on a few vertical levels. Total hail mass as a function of time is plotted in **Figure 4**

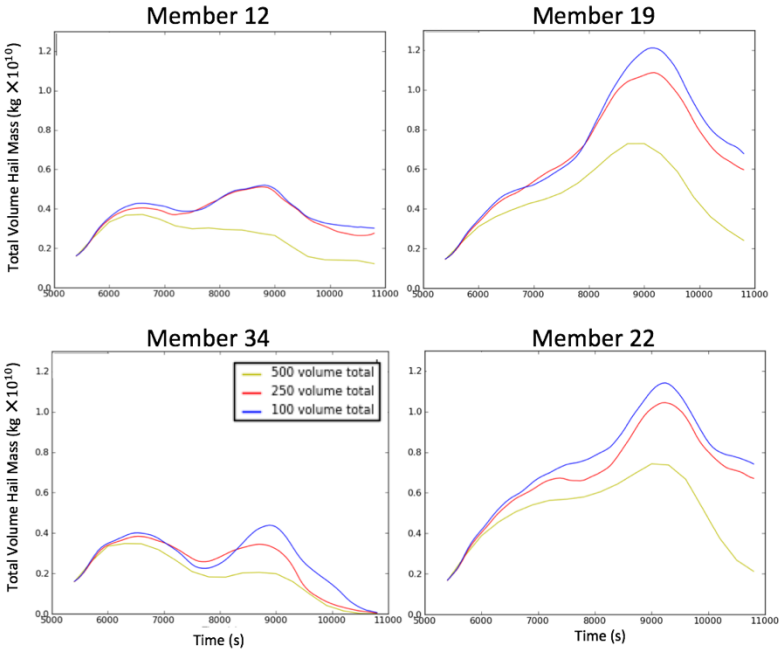

Figure 4: Total hail mass as a function of time for four ensemble members.

for four selected ensemble members. Ensemble members 12 and 34 were selected because they were among the lowest in terms of total hail mass produced at the surface; similarly, ensemble members 22 and 19 were selected because they were among the highest hail mass producers at the surface. In all four members considered, the 100m and 250m forecasts produced similar total hail mass throughout the forecast period, but also produced more hail than the 500m forecast at all times. The hail mass curves follow the same trend (in terms of increasing or decreasing hail mass production) at all grid spacings as the storm evolves. The 100m forecast does not always produce more total hail mass than the 250m forecast—values are often quite similar between the two runs, and 250m is occasionally slightly higher. In member 22, at the time of peak hail production, the 100m forecast produces higher total hail mass, while in member 19, the 250m forecast produces the highest. This is also seen in members 12 and 34, however large differences exist between the individual ensemble members in terms of total hail mass produced. The 500m forecasts do not produce as much hail mass as the 250m and 100m forecasts do in any member, which can be seen not only in the histograms but from the plots in **Figure 4**.

d. Vertical Cross Sections of Hail Mass

The structure of the hail cores will be analyzed qualitatively in this section using vertical cross sections taken in the east-west direction through the point where hail mass is highest at the surface. In **Figure 5**, the hail core of ensemble member 19 at time 7500s is plotted for the 500m, 250m, and 100m forecasts. A red line is plotted on the cross section indicating the position of the freezing level. Each cross section plot is 16 kilometers in width. A corresponding horizontal plot of radar reflectivity at the surface is shown for each vertical cross-section, with a red line indicating the location at which the cross section was taken.

In this member, large differences between the three grid spacings are evident. The 250m and 100m forecasts exhibit more intense hail cores and more hail aloft compared to the 500m forecast. Comparing the 250m and 100m forecasts, the width of the hail core is fairly similar, but the 100m forecast exhibits a larger area of very high hail mass within the hail core. This structure agrees with results from the histogram and swath analyses, in which large hail masses were more frequent and widespread in the 100m forecasts. Though this was the most frequent configuration, there were some ensemble members that produced similar

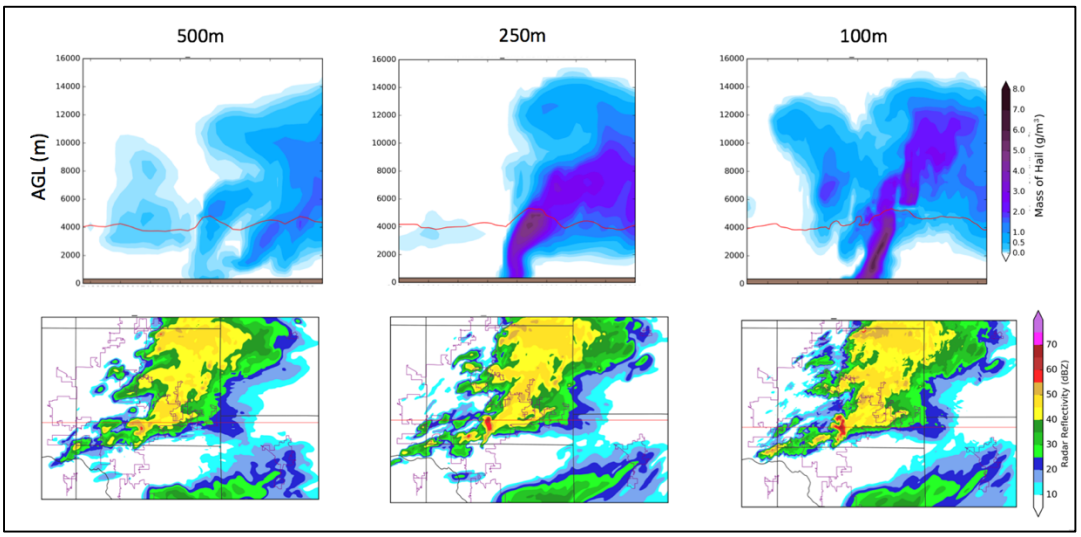

Figure 5: Vertical mass of hail cross section for ensemble member 19. Horizontal plots of model surface reflectivity at the time of the cross section are shown with a red line indicating the location of the cross section. Each vertical cross section is 16 kilometers in width.

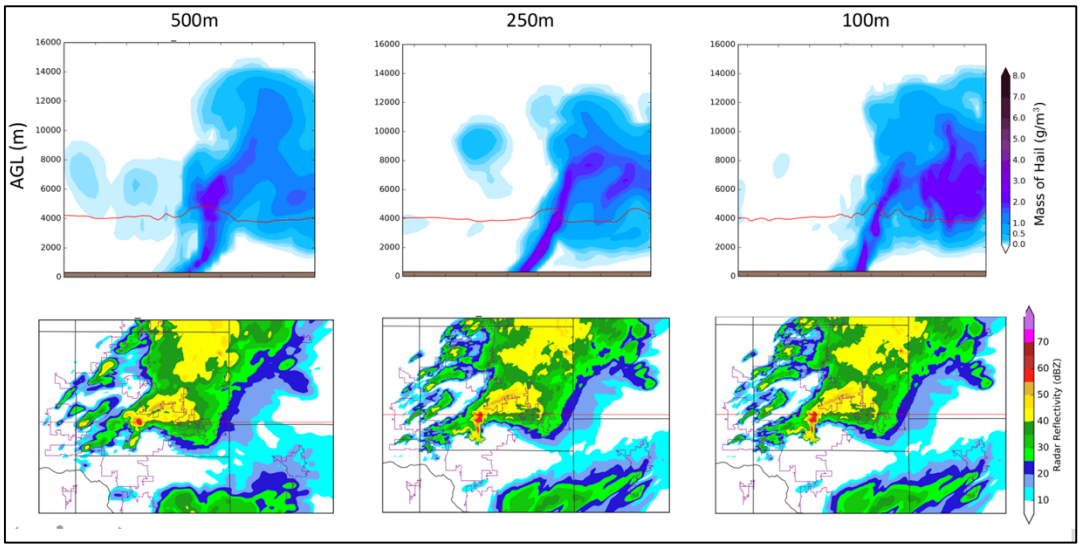

Figure 6: Mass of hail cross section similar to Figure 5 but for ensemble member 12.

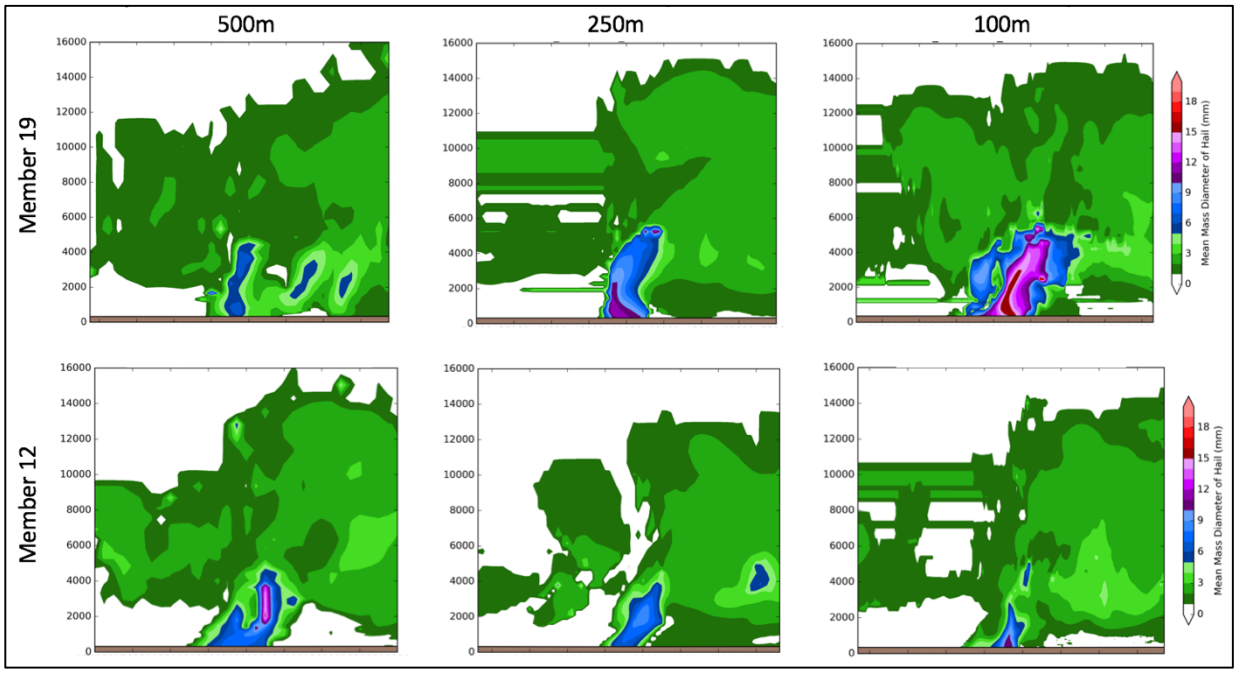

Figure 7: Vertical cross sections of hail mean mass diameter for ensemble members 19 and 12. Vertical axis is elevation above ground level in meters. Each vertical cross section is 16 kilometers in width.

structures and intensities in hail cores for all three forecasts, such as ensemble member 12 which is plotted in **Figure 6**. Between the three grid spacings for member 12, the hail shaft is similar in size and intensity, with the only considerable difference being the 100m has a larger quantity of higher hail mass in the upper levels around 6 kilometers, consistent with the mass of hail histogram results discussed earlier. In general, members that produced small amounts of total hail exhibited more similar structure within hail cores across grid spacings.

e. Analysis of Hail Mean Mass Diameter and Particle Size Distributions.

In the previous sections, the hail mass field was extensively examined to find quantitative and qualitative differences in hail production in the 500m, 250m, and 100m forecasts. However, mass of hail does not provide insight on concentrations of different sized hailstones or their distribution within the storm. For example, in the same cubic meter of volume, a mass of hail of 6 g m^{-3} could result from a large number of small hailstones or relatively few large hailstones. To make this comparison, mean-mass diameter (MMDI) and particle size distributions (PSDs) of hail are considered.

Mean mass diameter of hail is a derived variable that gives a good measurement of the diameter of hydrometeors in a specific grid volume. **Figure 7** shows MMDI for ensemble members 19 and 12. In ensemble member 19, at the surface and mid-levels, as the grid spacing is decreased, the model predicts larger hailstones and more widespread coverage of these larger hailstones. Member 12 exhibits a similar structure of mmdi between the 3 grid spacings, as it did for mass of hail, generally producing relatively little hail mass, as discussed in section d. The 100m forecast shows an area at the surface with moderate MMDI values, however in the 500m forecast, an area in the mid-levels can be seen with mmdi values upwards of 12mm, which is larger than in the 250m and 100m cross-sections. The trend in member 19 (with larger mmdi as grid spacing decreased) occurred more often compared to the trend in member 12, however both trends are shown to illustrate the variability in the field.

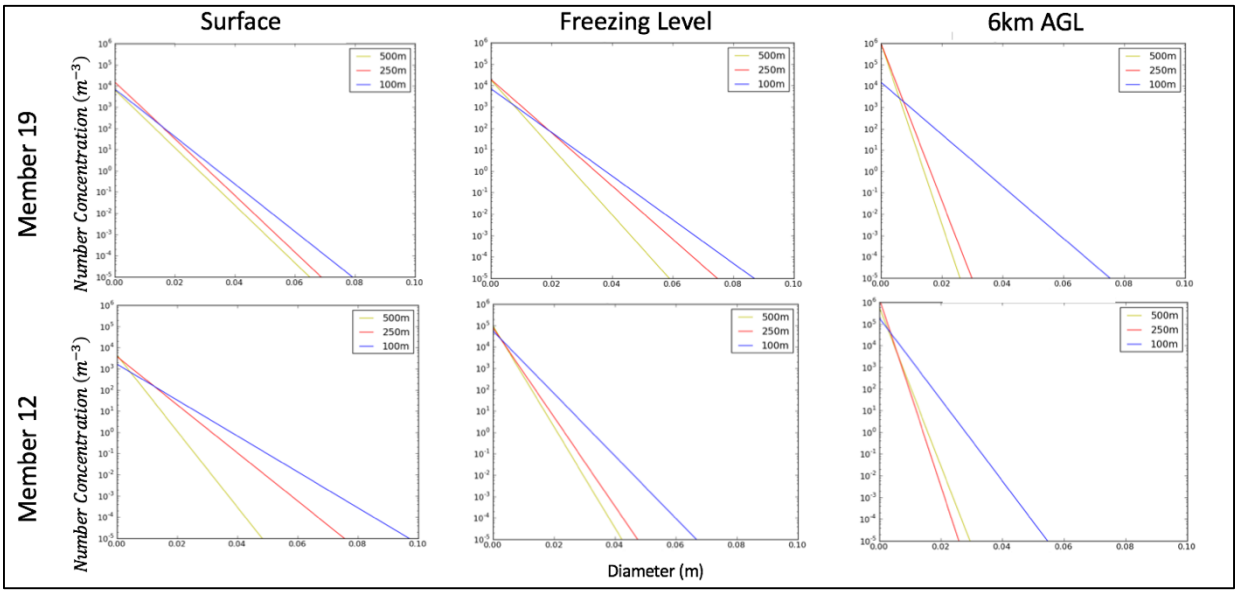

Figure 8: Particle size distributions for ensemble members 19 and 12 at the surface, freezing level, and 6 kilometer level.

Particle size distributions can be used as well to compare the concentrations of hailstones as a function of diameter. From the microphysical scheme used in these forecasts, the slope parameter and intercept parameter are explicitly predicted at each grid volume, allowing the gamma function (equation 1) to be plotted to show the number concentration of a certain hydrometeor as a function of diameter. From 6000 to 9000s of model time, the slope and intercept parameters are averaged at the grid volume of maximum mass of hail at each vertical level and for each grid spacing to obtain a representative average PSD curve. This method was necessary due to the large amount of spatial variation present in PSD curves within the hail cores—using an average allows for more insight on general trends. The resulting PSDs are shown in **Figure 8**.

For both members considered, a general trend is noticeable in the PSD curves: as grid spacing decreases, the slope of the PSD curve decreases, indicating a higher concentration of larger hailstones. This supports the analysis of mmdi results that suggested that as the grid spacing is decreased the number of larger diameter hailstones in the grid volume increases. The results from the qualitative analysis of mmdi and the quantitative analysis of PSD indicate that the differences seen in the mass of hail fields between the three grid spacings could be attributed to a difference in concentration of different hailstone sizes.

In the next three sections, we consider possible causes for the sensitivity of hail fields to grid spacing documented in the prior sections. We will examine updraft distributions, the near storm environment, and mass of graupel to identify differences in these related fields and whether such differences could possibly help to explain the source of the differences seen in the hail fields.

e. Updraft Distribution and Near Storm Environment

Updrafts play a large role in determining how large hailstones can grow, and because of this the distribution of updrafts is explored at the freezing level and at 6 kilometers above the surface. Histograms are produced and KS2 tests are performed in similar fashion as in section b. The histograms, along with the corresponding KS2 test results, are shown in **Figure 9**. Updraft bins are spaced at intervals of 1 m s^{-1} in the horizontal. The geographic distribution of updrafts are very similar at both the freezing level and 6 km above the surface; the only significant difference noted was for 50-70 m s^{-1} updrafts at the freezing level

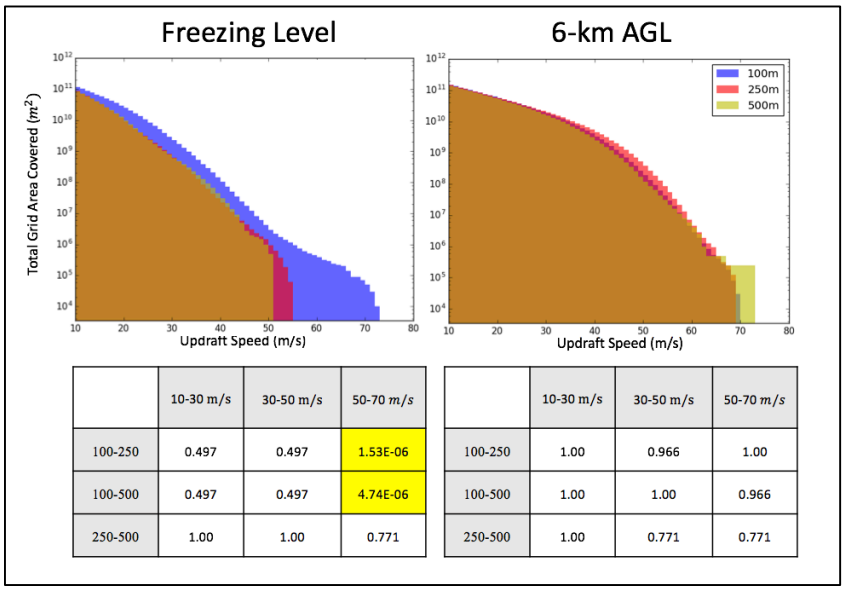

	10-30 m/s	30-50 m/s	50-70 m/s
100-250	0.497	0.497	1.53E-06
100-500	0.497	0.497	4.74E-06
250-500	1.00	1.00	0.771

	10-30 m/s	30-50 m/s	50-70 m/s
100-250	1.00	0.966	1.00
100-500	1.00	1.00	0.966
250-500	1.00	0.771	0.771

Figure 9: Updraft histograms for surface, freezing level, and 6 kilometers AGL. Updraft bins are spaced at intervals of 1 m s $^{-1}$ in the horizontal. Corresponding table of p values from Kolmogorov-Smirnov tests shown below histograms.

between the 100m forecast and the forecasts at the other two grid spacings.

Energy used to accelerate parcels within the updraft can also be generally associated with CAPE, which was compared across grid spacings and at several forecast times for member 12 in **Figure 10** to show the evolution of the near storm environment. No substantial differences were evident. The three grid spacings show similar CAPE fields, and similar modification of the near storm environment as the storm cools the surface and warms the air aloft, reducing CAPE values. This similar modification of the near storm environment was seen consistently throughout the ensemble members. Based on the near storm environment and the distribution of updrafts, it is likely that updraft speeds are not a major cause of the differences seen in the mass of hail field.

f. Mass of Graupel Distributions

Graupel serves as a source of hail embryos (Stensrud 2007), and therefore an analysis of graupel distribution is necessary to see if differences in the prediction of graupel are present which might impact the evolution of hail fields within the microphysical scheme. Similar to mass of hail and updraft fields, histograms are made along with results from a KS2 test with p values. The results of these tests are shown in **Figure 11**. Graupel mass bins are spaced at intervals of 0.1 g m^{-3} in the horizontal.

Interestingly, the trend in distributions seen in the mass of hail histogram for the freezing level is reversed for graupel. The 500m produces more geographic coverage of graupel across almost all ranges of mass, than the 250m followed by the 100m which produces the least amount of geographic coverage for all mass ranges. This same trend is not exactly seen in the histogram for the 6km level, however, for a large range of masses, the 250m produces more geographic coverage than the other two grid spacings. Comparing the mass of hail and mass of graupel histograms for the freezing level for the 100m and 500m forecasts, the 500m has more geographic coverage of graupel for all mass ranges while the 100m has more geographic coverage of hail mass. This suggests that greater conversion of hail to graupel might be present in the 100m forecast; additional microphysical budget analyses will be performed in the future to examine this possibility, but such analyses are beyond the scope of the current study.

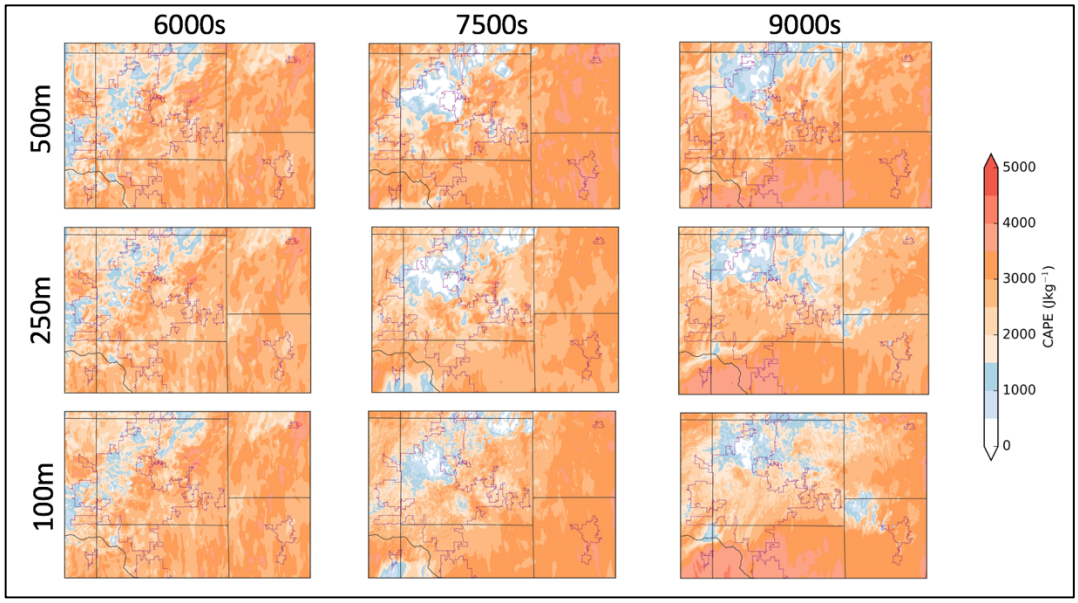

Figure 10: Horizontal plots of surface based convective available potential energy at several model times for ensemble member 12.

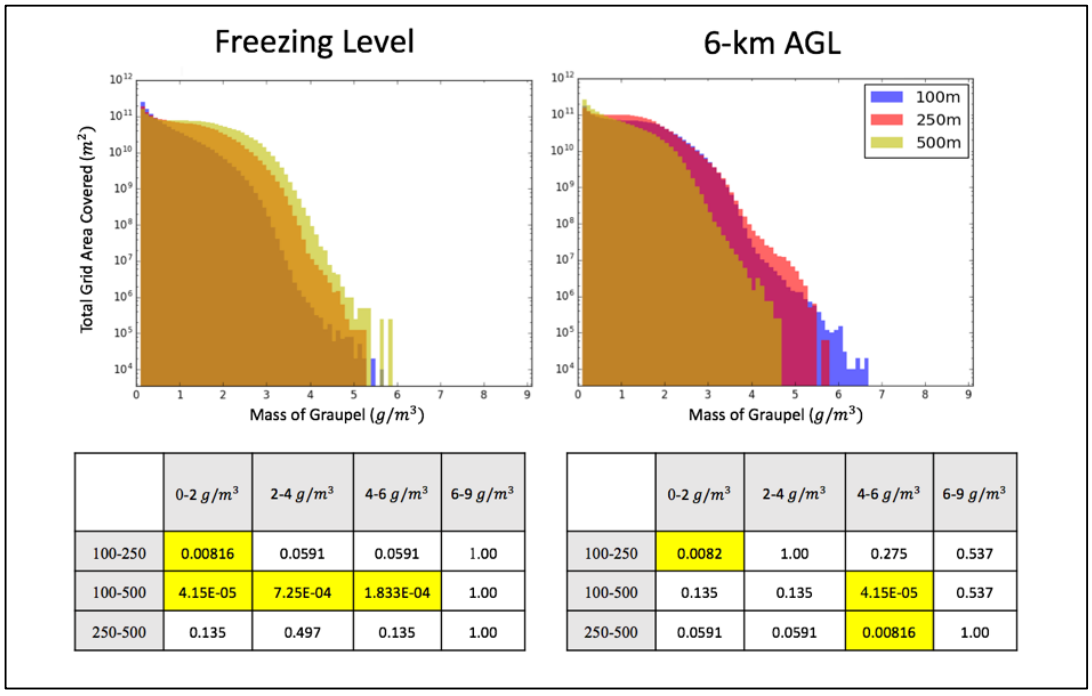

	0-2 g/m^3	2-4 g/m^3	4-6 g/m^3	6-9 g/m^3
100-250	0.00816	0.0591	0.0591	1.00
100-500	4.15E-05	7.25E-04	1.833E-04	1.00
250-500	0.135	0.497	0.135	1.00

	0-2 g/m^3	2-4 g/m^3	4-6 g/m^3	6-9 g/m^3
100-250	0.0082	1.00	0.275	0.537
100-500	0.135	0.135	4.15E-05	0.537
250-500	0.0591	0.0591	0.00816	1.00

Figure 11: Figure 3: Mass of graupel histograms for surface, freezing level, and 6 kilometers AGL. Graupel mass bins are spaced at intervals of 0.1 g m^{-3} in the horizontal. Corresponding table of p values from Kolmogorov-Smirnov are shown below histograms.

4. Summary and Discussion

In this study, the sensitivity of hail prediction to model grid spacing was investigated by identifying differences in the explicitly predicted mass of hail field as grid spacing was decreased from 500m to 250m to 100m. Any differences found were further investigated by analyzing related fields and variables such as the particle size distribution, distribution of updrafts and graupel, and the near storm environment to explore whether important differences in these fields existed, and if so, whether these differences were relevant to those found in the mass of hail field.

Systematic differences in the mass of hail field were found qualitatively through the use of hail swaths and vertical cross sections, and quantitatively through the use of histograms, statistical tests, and plots of total mass produced as a function of time for selected ensemble members. These results showed that as the grid spacing was decreased, the forecasts increased its spatial coverage of larger hail masses at the surface, freezing, and 6 kilometer AGL levels. The 100m forecast proved to be significantly different, using at KS2 significance test, in terms of hail mass distributions compared to the other two model grid spacings, for hail mass exceeding 4 g m^{-3}. In general, analysis of vertical cross sections of mass of hail confirmed the differences seen in the histograms and statistical tests, confirming that as the grid spacing decreased, larger mass of hail values were more frequently observed at the vertical levels considered.

Two related variables were considered in order to provide insight on the differences seen in the mass of hail field: near storm environment as measured by convective available potential energy, and updraft distribution. No significant differences were found in either of these two fields that were thought to have played an important role in the observed sensitivity of hail mass to grid spacing.

Differences were seen in the particle size distribution of hail and the graupel mass distribution. From the plots of PSD curves at the same vertical levels analyzed for the mass of hail histograms, a trend was noted: as the model grid spacing was decreased the concentration of larger hailstones increased. This is illustrated by the PSD curves in **Figure 8** decreasing in slope as the grid spacing became finer. This is an important difference because the mass of hail field does not directly give any information on the distribution of different sized hailstones—PSD diagrams can provide that information. This trend suggests that the differences in distribution of larger hail mass (greater than 4 grams per cubic meter) are likely accompanied by an increase in concentration of larger hailstones as the grid spacing is decreased.

The distribution of graupel also reinforces the findings of the PSD diagrams. It is shown in **Figure 11** that the trend of graupel mass as grid spacing decreases is the opposite of that noted for hail mass: as the grid spacing is decreased, there is less geographic coverage of graupel mass. This would suggest that the 100m and 250m forecasts might be converting more graupel embryos of all masses into hailstones. This would likely lead to larger growth of hailstones which causes larger mass of hail values to exist at these vertical levels. Detailed analysis of microphysical conversion terms within the model could further illuminate the observed behavior, and such future work is recommended.

Further analysis is needed on the sensitivity of hail to model grid spacing, possibly using model runs with smaller grid spacings still (e.g. 50 m), to see if the trends documented in this study are robust across different cases and microphysical schemes. The results of this study show that differences in the microphysical conversion terms within the model are likely to be the largest contributors to differences in hail prediction as the grid spacing varies (as differences in updraft structure and near-storm environment were largely ruled out by these results). Because of this, the focus of future work should be an analysis of the microphysical budget to examine whether differences within the microphysical budget and microphysical conversion terms can explain the differences in explicitly predicted hail fields in models with very fine grid spacing. This will be important for future operational use of models that can explicitly predict hail, especially if these models would use similar double moment bulk microphysical schemes.

Acknowledgments. This work was funded as part of the NSF Research Experience for

Undergraduates Program, Grant AGS-1560419. The data used in this study was a result of the SHARP project, supported by NSF Grant AGS-1261776. The authors thank John Labriola for his assistance with writing scripts and providing knowledge about the subject of hail prediction. The authors also would like to thank Tim Supinie for his help and expertise in scripting and working with data produced by the Advanced Regional Prediction System.

REFERENCES

Adams-Selin, R.D. and C.L. Ziegler, 2016: Forecasting Hail Using a One-Dimensional Hail Growth Model within WRF. *Mon. Wea. Rev.,* **144**, 4919–4939,https://doi.org/10.1175/MWR-D-16-0027.1

Adlerman, E. J. and Droegemeier, E. K., 2002: The sensitivity of Numerically Simulated Cyclic Mesoyclogenesis to Variations in Model Physical and Computational Parameters. *Mon. Wea. Rev., **130**, 2671-2691,doi: 10.1175/15200493(2002)130<2671:TSONSC>2.0.CO;2*

Allen, J.T, 2017: Atmospheric hazards: Hail potential heating up. *Nature Climate Change,* **7***,* 744-745*,* doi: 10.1038/nclimate3327

Bryan, G.H., J.C. Wyngaard, and J.M. Fritsch, 2003: Resolution Requirements for the Simulation of Deep Moist Convection. *Mon. Wea. Rev.,* **131**, 2394-2416, doi: https://doi.org/10.1175/1520-0493(2003)131<2394:RRFTSO>2.0.CO;2

Milbrandt, J. A., and Yau, M.K., 2005: A multimoment bulk microphysics parameterization. Part II: A proposed three-moment closure and scheme description. *J. Atmos. Sci.,* **62,** 3065-3081

NOAA, 2017: U.S. Billion-Dollar Weather & Climate Disasters 1980-2017. Accessed 10 July 2017. [Available online at http://www.ncdc.noaa.gov/billions/events.pdf]

Orf, L., R. Wilhelmson, B. Lee, C. Finley, and A. Houston, 2017: Evolution of a Long-Track Violent Tornado within a Simulated Supercell. *Bull. Amer. Meteor. Soc.,* **98**, 45–68, https://doi.org/10.1175/BAMS-D-15-00073.1

Snook, N., Jung, Y., Brotzge, J., Putnam, B., and Xue, M., 2016: Prediction and Ensemble Forecast Verification of Hail in the Supercell Storms of 20 May 2013. *Weather and Forecasting,* **31**, 811-825, doi: 10.1175/WAF-D-15-0152.1

Snook, N., Xue, M., and Jung, Y., 2015: Multiscale EnKF assimilation of radar and conventional observations and ensemble forecasting for a tornadic mesoscale convective system. *Mon. Wea. Rev.,* **143**, 1035-1057, doi:10.1175/MWR-D-13-00262.1.

Stensrud, D.J., 2007: *Parameterization Schemes: Keys to Understanding Numerical Weather Prediction Models.* Cambridge University Press, 459 pp.

Stensrud, D. J. and Coauthors, 2009: Convective-Scale Warn-on-Forecast System. *Bull. Amer. Meteor. Soc.,* **90,** 1487-1499, doi: 10.1175/2009BAMS2795.1

Tong, M. and M. Xue , 2008: Simultaneous estimation of microphysical parameters and atmospheric state with radar data and ensemble square root Kalman filter. Part I: Sensitivity analysis and parameter identifiability. Mon. Wea. Rev., 136, 1630–1648, doi:10.1175/2007MWR2070.1.

Xue, M., M. Tong, and K. K. Droegemeier, 2006: An OSSE framework based on the ensemble square root Kalman filter for evalu- ating the impact of data from radar networks on thunderstorm analysis and forecast. J. Atmos. Oceanic Technol., 23, 46–66, doi:10.1175/JTECH1835.1.

Zhang, Y., F. Zhang, D.J. Stensrud, and Z. Meng, 2015: Practical Predictability of the 20 May 2013 Tornadic Thunderstorm Event in Oklahoma: Sensitivity to Synoptic Timing and Topographical Influence. *Mon. Wea. Rev.,* **143**, 2973–2997, https://doi.org/10.1175/MWR-D-14-00394.1